Mechanics of Materials 42 (2010) 31–43

Contents lists available at ScienceDirect

Mechanics of Materials

journal homepage: www.elsevier.com/locate/mechmat

Thermomechanical analysis of steel cylinders quenching using a constitutive model with diffusional and non-diffusional phase transformations

Wendell Porto de Oliveira [a], Marcelo Amorim Savi [a,*], Pedro Manuel Calas Lopes Pacheco [b], Luís Felipe Guimarães de Souza [b]

[a] Universidade Federal do Rio de Janeiro, COPPE, Department of Mechanical Engineering, P.O. Box 68.503, 21.941.982 Rio de Janeiro, RJ, Brazil
[b] CEFET/RJ, Centro Federal de Educação Tecnológica Celso Suckow da Fonseca, Department of Mechanical Engineering, 20.271.110 Rio de Janeiro, RJ, Brazil

ARTICLE INFO

Article history:
Received 27 October 2008
Received in revised form 8 September 2009

Keywords:
Quenching
Phase transformation
Thermomechanical coupling
Modeling
Constitutive model
Numerical simulation
Experimental

ABSTRACT

Quenching is a commonly used heat treatment process employed to control the mechanical properties of steels. In brief, quenching consists of raising the steel temperature above a certain critical value, called austenitizing temperature, and then rapidly cooling it in a suitable medium to room temperature. The resulting microstructures formed from quenching (ferrite, cementite, pearlite, upper bainite, lower bainite and martensite) depend on cooling rate and on steel characteristics. This article deals with the themomechanical analysis of steel cylinder quenching. A multi-phase constitutive model is employed for its modeling and simulation. Experimental analysis related to temperature evolution during the process and its resulting microstructure is used as a reference for the modeling effort. The thermomechanical coupling terms of the energy equation are included in the formulation. The through hardening of a cylindrical body is considered as an application of the proposed general formulation. Numerical simulations present good agreements with experimental data, indicating the model capability to capture the general thermomechanical behavior of the quenching process.

1. Introduction

Quenching is a heat treatment usually employed in industrial processes in order to control mechanical properties of steels as toughness and hardness. The process consists of raising the steel temperature above a certain critical value, holding it at that temperature for a specified time and then rapidly cooling it in a suitable medium to room temperature. The resulting microstructures formed from quenching (ferrite, cementite, pearlite, upper bainite, lower bainite and martensite) depend on cooling rate and on chemical composition of the steel. The volume expansion associated with the formation of martensite combined with large temperature gradients and non-uniform cooling can promote high residual stresses. Since these internal stresses can produce warping and even cracking of a steel body, the prediction of such stresses is an important task.

Phenomenological aspects of quenching involve couplings among different physical processes and its description is unusually complex. Basically, three couplings are essential: thermal, phase transformation and mechanical phenomena. The description of each one of these phenomena has been addressed by several authors by considering these aspects separately. Sen et al. (2000) considered steel cylinders without phase transformations. There are also references focused on the modeling of the phase transformation phenomenon (Hömberg, 1996; Chen et al., 1997; Çetinel et al., 2000; Reti et al., 2001). Several authors have proposed coupled models that are usually applicable to

* Corresponding author.
E-mail addresses: wendell@furnas.com.br (W.P. de Oliveira), savi@mecanica.ufrj.br (M.A. Savi), calas@cefet-rj.br (P.M.C.L. Pacheco), lfelipe@cefet-rj.br (L.F.G. de Souza).

0167-6636/$ - see front matter © 2009 Elsevier Ltd. All rights reserved.
doi:10.1016/j.mechmat.2009.09.006

simple geometries as cylinders (Inoue and Wang, 1985; Melander, 1985; Sjöström, 1985; Denis et al., 1985, 1987, 1999; Denis, 1996; Fernandes et al., 1985; Woodard et al., 1999; Ju et al., 2006). Moreover, there are some complex aspects that are usually neglected in the analysis of quenching process. For example, one could mention the heat generated during phase transformation, transformation induced plasticity and volumetric expansion associated with phase transformation. The heat generated during phase transformation is usually treated by means of the latent heat associated with phase transformation (Inoue and Wang, 1985; Denis et al., 1987, 1999; Sjöström, 1994; Woodard et al., 1999). Meanwhile, other coupling terms in the energy equation related to other phenomena as plastic strain or hardening are not treated in literature and their analysis is an important topic to be investigated. Silva et al. (2004) analyzed the thermomechanical coupling during quenching considering austenite-martensite phase transformations. Afterwards, Silva et al. (2005) employed the finite element method to the quenching analysis. Kang and Im (2007a,b,c) presented a modeling effort employing the finite element model to perform numerical simulations. Results are in close agreement with experimental tests available in literature. Sinha et al., (2007) and Huiping et al. (2007) are others interesting contributions considering multi-phase models.

This article deals with the themomechanical analysis of steel cylinder quenching. A multi-phase constitutive model is employed for its modeling and simulation. Diffusional and non-diffusional phase transformations are considered in the formulation. Experimental analysis related to temperature evolution during the process and its resulting microstructure is used as a reference for the modeling effort. The kinetics of the diffusive transformations is described by the Johnson, Mehl, Avrami and Kolmogorov (JMAK) law (Avrami, 1940; Cahn, 1956), while non-diffusive transformations are described by the Koistinen–Marburger law. The thermomechanical coupling terms of the energy equation are analyzed considering the latent heat associated with phase transformation. This model is a first approach to represent thermomechanical couplings in the energy equation associated with phase transformation, plasticity and hardening, allowing the investigation of the effects promoted by these coupling (Silva et al., 2004).

A numerical procedure is developed based on the operator split technique (Ortiz et al., 1983) associated with an iterative numerical scheme in order to deal with nonlinearities in the formulation. Under this assumption, the coupled governing equations are solved from four uncoupled problems: thermal, phase transformation, thermoelastic and elastoplastic. The proposed general formulation is applied to the through hardening of steel cylinders. Numerical results show that the proposed model is capable of capturing the general behavior observed on experimental data. Besides, numerical results present a good agreement with those of experimental data (Oliveira et al., 2003; Oliveira, 2004).

2. Phenomenological aspects of phase transformations

Quenching of steel is the rapid cooling of steel heated to the austenitizing temperature. Depending on the cooling rate imposed by the type of quenching medium and chemical composition of the steel, transformation of the austenite phase into different microstructures can arise as: ferrite, cementite, pearlite, upper bainite, lower bainite and martensite. In order to deal with all these microstructures in a macroscopic point of view, the volume fraction of each one of these phases is represented by β_m (austenite $m = 0$, ferrite $m = 1$, cementite $m = 2$, pearlite $m = 3$, upper bainite $m = 4$, lower bainite $m = 5$ and martensite $m = 6$). All of these phases may coexist, satisfying the following constraints: $\sum_{m=0}^{6}\beta_m = 1$ and $0 \leqslant \beta_m \leqslant 1$ $(m = 1, .., 6)$, where $\beta_0 = \beta_A$ and $\beta_6 = \beta_M$. Reverse transformations from parent to the austenitic phase ($\beta_m \rightarrow \beta_A$; $m = 1, .., 6$), which occurs during heating, are not considered.

Phase transformation from austenite to martensite is a non-diffusive process, which means that the amount of volume fraction is only a function of temperature (Chen et al., 1997; Çetinel et al., 2000; Reti et al., 2001). This process may be described by the equation proposed by Koistinen and Marburger (1959),

$$\beta_M = \beta_A^0[1 - e^{-k(M_s - T)}] \tag{1}$$

where β_A^0 is the amount of austenite at the beginning of martensitic transformation, k is a material property and T is the temperature. Under a stress-free state, M_s and M_f are the temperatures where martensitic transformation starts and finishes its formation. Assuming M_f as the temperature where martensitic phase reaches an amount of 99%, from Eq. (1), $k = 2\ln(10)/(M_s - M_f)$. In order to incorporate these limits in Eq. (1) and also to assure that the martensite transformation only occurs during cooling, the following condition is defined by using the Heaviside function, $\Gamma(x)$, (Hömberg, 1996; Chen et al., 1997):

$$\varsigma_{A\rightarrow M}(\dot{T}, T) = \Gamma(-\dot{T})\Gamma(M_s - T)\Gamma(T - M_f) \tag{2}$$

where dot represents the differentiation with respect to time t. Therefore, the evolution of martensitic phase can be rewritten in a rate form as follows:

$$\dot{\beta}_M = \varsigma_{A\rightarrow M}\beta_A^0[(1 - \beta_M)k\dot{T}] \tag{3}$$

Pearlite, cementite, ferrite and bainite formations are diffusion-controlled transformations, which mean that they are time dependent. The evolution of these phase transformations can be predicted through an approximate solution using data from Time–Temperature-Transformation diagrams (TTT) (Çetinel et al., 2000; Reti et al., 2001). The analysis of phase transformation using this diagram is done by assuming that the cooling process may be represented by a curve divided in a sequence of isothermal steps, with a duration Δt, as shown in the Continuous-Cooling-Transformation diagram (CCT) of Fig. 1a. Through each isothermal step, the phase evolution is calculated by considering isothermal transformation kinetics expressed by the JMAK law (Avrami, 1940; Cahn, 1956; Çetinel et al., 2000; Reti et al., 2001):

$$\beta_m(t) = \hat{\beta}_m^{\max}[1 - e^{-b_m(t)^{N_m}}] \quad (m = 1, \ldots, 5) \tag{4}$$

where

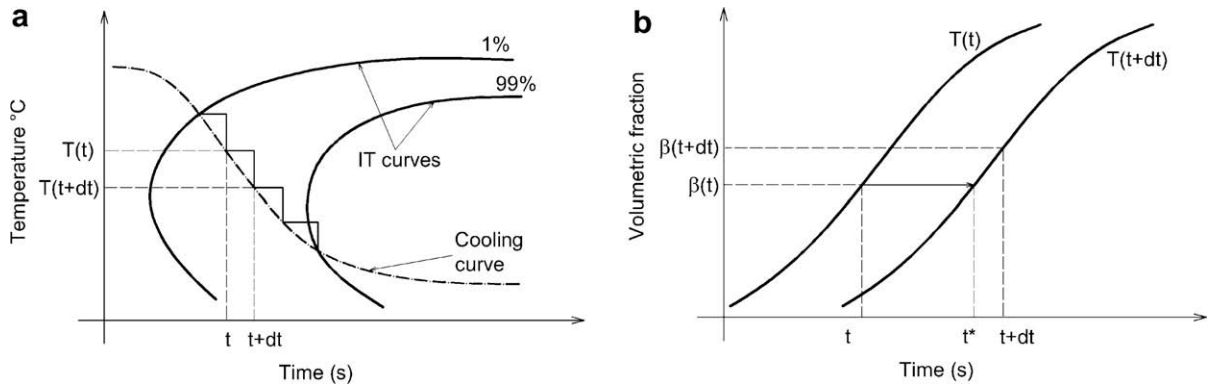

Fig. 1. (a) Cooling curve represented in a CCT diagram by a series of small isothermal time steps and (b) fictitious time.

$$N_m = \frac{6.1273}{\ln\left(\frac{t_m^f}{t_m^s}\right)}; \quad b_m = \frac{0.01005}{(t_m^s)^{N_m}} \tag{5}$$

Note that β_m is the volume fraction of m-phase, at a constant temperature T during the time t, measured from the start of cooling process; N_m is the Avrami exponent and b_m is a parameter that characterizes the rate of nucleation and growth processes (Avrami, 1940; Reti et al., 2001). The parameter $\hat{\beta}_m^{\max}$ is represented by

$$\hat{\beta}_m^{\max} = \beta_m^{\max}\left[1 - \left(\sum_{j=1;j\neq m}^{5} \beta_j\right) - \beta_M\right] \quad (m = 1,\ldots,5) \tag{6}$$

where $\beta_m^{\max}$ represents the maximum volume fraction for an m-phase. These three parameters are temperature functions and can be obtained from TTT diagrams being usually fitted from experimental curves (Hömberg, 1996; Çetinel et al., 2000; Reti et al., 2001).

At this point, it should be pointed out that Eq. (4) is valid for an isothermal transformation and therefore, it must be modified to be applied to an anisothermal process. This is done approximating the anisothermal process by a sequence of isothermal steps shown in Fig. 1a. Therefore, a fictitious time t^* is defined, including effects associated with temperature change from step T to step $(T + \Delta T)$. Under this assumption, the fictitious time t^* represents the time for the formation of the volume fraction β_m at temperature T, considering an isothermal transformation developed at temperature $(T + \Delta T)$. This definition is considered as follows:

$$t^* = \left[-\frac{1}{b_m(T+\Delta T)}\ln\left(1 - \frac{\beta_m(T)}{\hat{\beta}_m^{\max}(T+\Delta T))}\right)\right]^{\frac{1}{N_m(T+\Delta T)}} \quad (m = 1,\ldots,5) \tag{7}$$

This fictitious time is used as the starting point to compute the phase evolution during the isothermal time step Δt at temperature $(T + \Delta T)$, as shown in Fig. 1b. Now, the amount of volume fraction at the end of the isothermal step $(T + \Delta T)$, at the time instant $(t + \Delta t)$, can be computed as follows (Çetinel et al., 2000; Reti et al., 2001):

$$\beta_m(T+\Delta T) = \hat{\beta}_m^{\max}(T+\Delta T) \times\left[1 - e^{-b_m(T+\Delta T)(t^*+\Delta t)^{N_m(T+\Delta T)}}\right] \quad (m=1,\ldots,5) \tag{8}$$

Moreover, it is important to define a condition that incorporates the temperature dependent functions and also assure its irreversibility:

$$\varsigma_{A\to phase\,(m)}(\dot{T},t) = \Gamma(-\dot{T})\,\Gamma(t_m^f - t)\Gamma(t - t_m^s)(m = 1,\ldots,5) \tag{9}$$

where t_m^s and t_m^f limit the start and finish of the phase transformation.

Under these assumptions, the rate form of m-phase volume fraction is written as follows,

$$\dot{\beta}_m = \varsigma_{A\to phase(m)}\left\{N_m(b_m)^{(1/N_m)}(\hat{\beta}_m^{\max} - \beta_m)\left[\ln\left(\frac{\hat{\beta}_m^{\max}}{\hat{\beta}_m^{\max} - \beta_m}\right)\right]^{\left(1-\frac{1}{N_m}\right)}\right\} \quad (m=1,\ldots,5) \tag{10}$$

3. Constitutive model

Constitutive equations may be formulated within the framework of continuum mechanics and the thermodynamics of irreversible processes, by considering thermodynamic forces, defined from the Helmholtz free energy, ψ, and thermodynamic fluxes, defined from the pseudo-potential of dissipation, φ (Pacheco et al., 2001).

The proposed phenomenological quenching model allows one to identify different aspects related to quenching process. With this aim, a Helmholtz free energy is proposed as a function of observable variables: total strain, ε_{ij}, and temperature, T. Moreover, the following internal variables are considered: plastic strain, ε_{ij}^p, kinematic hardening, α_{ij}, volumetric strain associated with phase transformation from a parent phase, ε_{ij}^{tv}, transformation plasticity strain, ε_{ij}^{tp}, and the volume fractions of seven different microstructures: β_m $(m = 0,\ldots,6)$ (respectively, austenite, ferrite, cementite, pearlite, upper bainite, lower bainite and martensite). Alternatively, it is used: $\beta_0 = \beta_A$ and $\beta_6 = \beta_M$.

Under these assumptions, the Helmholtz free energy density for each m-phase is defined as follows:

$$\rho\psi^{(m)}(\varepsilon_{ij},\varepsilon^{p}_{ij},\alpha_{ij},\varepsilon^{tv}_{ij},\varepsilon^{tp}_{ij},T) = W^{(m)}(\varepsilon_{ij},\varepsilon^{p}_{ij},\alpha_{ij},\varepsilon^{tv}_{ij},\varepsilon^{tp}_{ij},T) = W^{(m)}_{e}(\varepsilon_{ij},\varepsilon^{p}_{ij},\varepsilon^{tv}_{ij},\varepsilon^{tp}_{ij},T) + W^{(m)}_{\alpha}(\alpha_{ij}) - W^{(m)}_{T}(T) \quad (11)$$

The free energy density for each phase is expressed by the following expressions:

$$W^{(m)}_{e}(\varepsilon_{ij},\varepsilon^{p}_{ij},\varepsilon^{tv}_{ij},\varepsilon^{tp}_{ij}) = \frac{1}{2}E^{(m)}_{ijkl}\left[\varepsilon_{ij}-\varepsilon^{p}_{ij}-\alpha^{(m)}_{T}(T-T_0)\delta_{ij} - \varepsilon^{tv}_{ij}-\varepsilon^{tp}_{ij}\right]\left[\varepsilon_{kl}-\varepsilon^{p}_{kl}-\alpha^{(m)}_{T}(T-T_0)\delta_{kl}-\varepsilon^{tv}_{kl}-\varepsilon^{tp}_{kl}\right] \quad (12)$$

$$W^{(m)}_{\alpha}(\alpha_{ij}) = \frac{1}{2}H^{(m)}_{ijkl}\alpha_{ij}\alpha_{kl} \quad (13)$$

$$W^{(m)}_{T}(T) = \rho\int_{T_0}^{T} C^{(m)}_{1}\log(\xi)d\xi + \frac{\rho}{2}C^{(m)}_{2}T^2 \quad (14)$$

where $E^{(m)}$ is the Young modulus and $H^{(m)}$ is the hardening modulus related to the m-phase; ρ is the material density; $C^{(m)}_1$ and $C^{(m)}_2$ are constants related to the m-phase. The increment of elastic strain is defined by assuming an additive decomposition:

$$d\varepsilon^{e}_{ij} = d\varepsilon_{ij} - d\varepsilon^{p}_{ij} - \left(\sum_{m=0}^{6}\beta_m\alpha^{(m)}_{T}\right)dT\delta_{ij} - d\varepsilon^{tv}_{ij} - d\varepsilon^{tp}_{ij} \quad (15)$$

Eq. (15) defines the increment of elastic strain (left hand side). In the right hand side, the first term is the total strain while the second is related to plastic strain. The third term is associated with thermal expansion. The parameter $\alpha^{(m)}_T$ is the coefficient of linear thermal expansion related to the m-phase, δ_{ij} is the Kronecker delta. The fourth term is related to volumetric expansion associated with phase transformation from a parent phase $d\varepsilon^{tv}_{ij} = \left(\sum_{m=1}^{6}\gamma^{(m)}d\beta_m\right)\delta_{ij}$, where $\gamma^{(m)}$ is a material property related to total expansion. Finally, the last term is denoted as transformation plasticity strain $d\varepsilon^{tp}_{ij} = \sum_{m=1}^{6}\frac{3}{2}\kappa^{(m)}f'(\beta_m)\,d\beta_m\sigma^{d}_{ij}$, being the result of several physical mechanisms related to local plastic strain promoted by the phase transformation (Denis et al., 1985; Sjöström, 1985); $\kappa^{(m)}$ is a material parameter, $f(\beta_m)$ expresses the transformation process dependence and σ^{d}_{ij} is the deviatoric stress defined by $\sigma^{d}_{ij} = \sigma_{ij} - \delta_{ij}(\sigma_{kk}/3)$, with σ_{ij} being the stress tensor component. It should be emphasized that this plastic strain may be related to stress states that are inside the yield surface.

A free energy density of the mixture can be written as follows:

$$\rho\psi\left(\varepsilon_{ij},\varepsilon^{p}_{ij},\alpha_{ij},\varepsilon^{tv}_{ij},\varepsilon^{tp}_{ij},T,\beta_0,\beta_1,\beta_2,\beta_3,\beta_4,\beta_5,\beta_6\right) = W\left(\varepsilon_{ij},\varepsilon^{p}_{ij},\alpha_{ij},\varepsilon^{tv}_{ij},\varepsilon^{tp}_{ij},T,\beta_0,\beta_1,\beta_2,\beta_3,\beta_4,\beta_5,\beta_6\right) = \sum_{m=0}^{6}\beta_m W^{(m)}\left(\varepsilon_{ij},\varepsilon^{p}_{ij},\alpha_{ij},\varepsilon^{tv}_{ij},\varepsilon^{tp}_{ij},T\right) + W_{\beta}(\beta_0,\beta_1,\beta_2,\beta_3,\beta_4,\beta_5,\beta_6) \quad (16)$$

where $W_\beta(\beta_0,\beta_1,\beta_2,\beta_3,\beta_4,\beta_5,\beta_6) = J_\pi(\beta_0,\beta_1,\beta_2,\beta_3,\beta_4,\beta_5,\beta_6)$ represents the indicator function associated with the following convex set π:

$$\pi = \left\{\beta_m \in \Re | 0 \le \beta_m \le 1\ (m = 0,1,\ldots 6);\ \sum_{m=0}^{6}\beta_m = 1\right\} \quad (17)$$

At this moment, it is possible to define the energy functions as follows:

$$W_e\left(\varepsilon_{ij},\varepsilon^{p}_{ij},\varepsilon^{tv}_{ij},\varepsilon^{tp}_{ij},T,\beta_0,\beta_1,\beta_2,\beta_3,\beta_4,\beta_5,\beta_6\right) = \frac{1}{2}\left\{\sum_{m=0}^{6}\beta_m E^{(m)}_{ijkl}\left[\varepsilon_{ij}-\varepsilon^{p}_{ij}-\alpha^{(m)}_{T}(T-T_0)\delta_{ij}-\varepsilon^{tv}_{ij}-\varepsilon^{tp}_{ij}\right] \times\left[\varepsilon_{kl}-\varepsilon^{p}_{kl}-\alpha^{(m)}_{T}(T-T_0)\delta_{kl}-\varepsilon^{tv}_{kl}-\varepsilon^{tp}_{kl}\right]\right\} \quad (18)$$

$$W_\alpha(\alpha_{ij},\beta_0,\beta_1,\beta_2,\beta_3,\beta_4,\beta_5,\beta_6) = \frac{1}{2}\left[\sum_{m=0}^{6}\beta_m H^{(m)}_{ijkl}\right]\alpha_{ij}\alpha_{kl} \quad (19)$$

$$W_\beta(\beta_0,\beta_1,\beta_2,\beta_3,\beta_4,\beta_5,\beta_6) = J_\pi(\beta_0,\beta_1,\beta_2,\beta_3,\beta_4,\beta_5,\beta_6) \quad (20)$$

$$W_T(T,\beta_0,\beta_1,\beta_2,\beta_3,\beta_4,\beta_5,\beta_6) = \rho\int_{T_0}^{T}\left[\sum_{m=0}^{6}\beta_m C^{(m)}_1\right] \times\ \log(\xi)d\xi + \frac{\rho}{2}\left[\sum_{m=0}^{6}\beta_m C^{(m)}_2\right]T^2 \quad (21)$$

Therefore, the generalized standard material approach establishes the following definitions of the thermodynamical forces $(\sigma_{ij}, P_{ij}, X_{ij}, Q_{ij}, R_{ij}, s, B^{\beta_1}, B^{\beta_2}, B^{\beta_3}, B^{\beta_4}, B^{\beta_5}, B^{\beta_6})$, associated with state variables $(\varepsilon_{ij}, \varepsilon^{p}_{ij}, \alpha_{ij}, \varepsilon^{tv}_{ij}, \varepsilon^{tp}_{ij}, T, \beta_0, \beta_1, \beta_2, \beta_3, \beta_4, \beta_5, \beta_6)$:

$$\sigma_{ij} = \frac{\partial W}{\partial\varepsilon_{ij}} = \sum_{m=0}^{6}\beta_m E^{(m)}_{ijkl}[\varepsilon_{kl}-\varepsilon^{p}_{kl}-\alpha^{(m)}_{T}(T-T_0) \delta_{kl}-\varepsilon^{tv}_{kl}-\varepsilon^{tp}_{kl}] \quad (22)$$

$$P_{ij} = -\frac{\partial W}{\partial\varepsilon^{p}_{ij}} = \sigma_{ij} \quad (23)$$

$$X_{ij} = \frac{\partial W}{\partial\alpha_{ij}} = \left[\sum_{m=0}^{6}\beta_m H^{(m)}_{ijkl}\right]\alpha_{kl} \quad (24)$$

$$Q_{ij} = -\frac{\partial W}{\partial\varepsilon^{tv}_{ij}} = \sigma_{ij} \quad (25)$$

$$R_{ij} = -\frac{\partial W}{\partial\varepsilon^{tp}_{ij}} = \sigma_{ij} \quad (26)$$

$$s = -\frac{1}{\rho}\frac{\partial W}{\partial T} \quad (27)$$

$$B^{\beta_m} = -\frac{\partial W}{\partial\beta_m} \in -\partial_{\beta_m}J_\pi - \left[\frac{\partial W_e}{\partial\beta_m}+\frac{\partial W_\alpha}{\partial\beta_m}+\frac{\partial W_T}{\partial\beta_m}\right] \quad \text{for} \quad (m = 1,\ldots,6) \quad (28)$$

where $\partial_{\beta_m}J_\pi$ is the sub-differential of the indicator function J_π.

In order to describe dissipation processes, it is necessary to introduce a potential of dissipation or its dual, which can be split into internal and thermal parts:

$$\phi^*(P_{ij},Q_{ij},R_{ij},X_{ij},B^{\beta_1},B^{\beta_2},B^{\beta_3},B^{\beta_4},B^{\beta_5},B^{\beta_6},g_i) = \phi^*_I(P_{ij},Q_{ij},R_{ij},X_{ij},B^{\beta_1},B^{\beta_2},B^{\beta_3},B^{\beta_4},B^{\beta_5},B^{\beta_6}) + \phi^*_T(g_i) \quad (29)$$

$$\begin{cases}\phi^*_I = I^*_v(P_{ij},X_{ij}) + \sum_{m=1}^{6}\gamma^{(m)}\dot\beta_m Q_{ij} \\ + \sum_{m=1}^{6}\frac{3\kappa^{(m)}\dot\beta_m f'(\beta_m)}{4}\left(R_{ij}-\frac{R_{kk}}{3}\delta_{ij}\right)\left(R_{ij}-\frac{R_{kk}}{3}\delta_{ij}\right) + \sum_{m=1}^{6}B^{\beta_m}\dot\beta_m \\ \phi^*_T = \frac{T}{2}\left[\sum_{m=0}^{6}\beta_m\Lambda^{(m)}\right]g_i g_i\end{cases} \quad (30)$$

where $g_i = (1/T)\partial T/\partial x_i$ and $\Lambda^{(m)}$ is the thermal conductivity coefficient related to the m-phase, that is function of temperature; $I^*_v(P_{ij}, X_{ij})$ is the indicator function associated with elastic domain, related to the *von Mises* criterion (Lemaitre and Chaboche, 1990),

$$v(P_{ij}, X_{ij}) = \left[\frac{3}{2}(P^d_{ij} - X^d_{ij})(P^d_{ij} - X^d_{ij})\right]^{1/2} - \left[\sum_{m=0}^{6} \beta_m S^{(m)}_Y\right] \leq 0 \tag{31}$$

$S^{(m)}_Y$ is the material yield stress, related to the m-phase, $X^d_{ij} = X_{ij} - \delta_{ij}(X_{kk}/3)$ and $P^d_{ij} = \sigma^d_{ij}$.

Under this assumption, the generalized standard material approach establishes the following definitions of the thermodynamic fluxes, expressed as evolution laws obtained from ϕ^*:

$$\dot{\varepsilon}^p_{ij} \in \partial_{P_{ij}} I^*_v(P_{ij}, X_{ij}) = \lambda \operatorname{sign}\left(\sigma_{ij} - \left[\sum_{m=0}^{6} \beta_m H^{(m)}_{ijkl}\right]\alpha_{kl}\right) \tag{32}$$

$$\dot{\alpha}_{ij} \in -\partial_{X_{ij}} I^*_v(\sigma_{ij}, X_{ij}) = \dot{\varepsilon}^p_{ij} \tag{33}$$

$$\dot{\varepsilon}^{tv}_{ij} = \frac{\partial \phi^*}{\partial Q_{ij}} = \sum_{m=1}^{6} \gamma^{(m)} \dot{\beta}_m \delta_{ij} \tag{34}$$

$$\dot{\varepsilon}^{tp}_{ij} = \frac{\partial \phi^*}{\partial R_{ij}} = \sum_{m=1}^{6} \frac{3}{2} \kappa^{(m)} f'(\beta_m) \dot{\beta}_m \sigma^d_{ij} \tag{35}$$

$$\dot{\beta}_M = \frac{\partial \phi^*}{\partial B^{\beta_M}} = \varsigma_{A\to M} \beta^0_A [(1 - \beta_M) k \dot{T}] \tag{36}$$

$$\dot{\beta}_m = \frac{\partial \phi^*}{\partial B^{\beta_m}} = \varsigma_{A\to m} \left\{ N_m (b_m)^{(1/N_m)} (\hat{\beta}^{\max}_m - \beta_m) \times \left[\ln\left(\frac{\hat{\beta}^{\max}_m}{\hat{\beta}^{\max}_m - \beta_m}\right)\right]^{\left(1-\frac{1}{N_m}\right)} \right\} \quad (m = 1, .., 5) \tag{37}$$

$$q_i = -\frac{\partial \phi^*}{\partial g_i} = -\left[\sum_{m=0}^{6} \beta_m \Lambda^{(m)}\right] T g_i = -\left[\sum_{m=0}^{6} \beta_m \Lambda^{(m)}\right] \frac{\partial T}{\partial x_i} \tag{38}$$

where $\operatorname{sign}(x) = x/|x|$, λ is the plastic multiplier from the classical theory of plasticity (Lemaitre and Chaboche, 1990) and q_i is the heat flux vector. By assuming that the specific heat is $\left[\sum_{m=0}^{6} \beta_m c^{(m)}\right] = -(T/\rho)\partial^2 W/\partial T^2$ and the set of constitutive Eqs. (22)–(28), (32)–(38), the energy equation can be written as (Pacheco, 1994):

$$\frac{\partial}{\partial x_i}\left(\left[\sum_{m=0}^{6} \beta_m \Lambda^{(m)}\right] \frac{\partial T}{\partial x_i}\right) - \rho \left[\sum_{m=0}^{6} \beta_m c^{(m)}\right] \dot{T} = -a_I - a_T \tag{39}$$

where

$$a_I = \sum_{m=1}^{6} B^{\beta_m} \dot{\beta}_m - X_{ij} \dot{\varepsilon}^p_{ij} + \sigma_{ij}(\dot{\varepsilon}^p_{ij} + \dot{\varepsilon}^{tv}_{ij} + \dot{\varepsilon}^{tv}_{ij}) \tag{40}$$

$$a_T = T\left[\frac{\partial \sigma_{ij}}{\partial T}(\dot{\varepsilon}_{ij} - \dot{\varepsilon}^p_{ij} - \dot{\varepsilon}^{tp}_{ij} - \dot{\varepsilon}^{tv}_{ij}) - \sum_{m=1}^{6} \frac{\partial B^{\beta_m}}{\partial T} \dot{\beta}_m + \frac{\partial X_{ij}}{\partial T} \dot{\varepsilon}^p_{ij}\right] \tag{41}$$

The preceding expressions of a_I and a_T represent internal and thermal coupling, respectively. The thermomechanical coupling effect related to phase transformation may be represented as a latent heat released during the phase transformation (Fernandes et al., 1985; Denis et al., 1987; Woodard et al., 1999):

$$a_I + a_T = \dot{Q} = \sum_{m=1}^{6} \Delta H^{(m)} \dot{\beta}_m \tag{42}$$

where $\Delta H^{(m)}$ is the enthalpy variation in a transformation process involving a previous phase (austenite) and a product phase β_m ($m = 1, \ldots, 6$). Therefore, this source term is used instead of all thermomechanical coupling effects, which represents a first approach of the general formulation (Silva et al., 2004).

Moreover, boundary conditions may be expressed as follows:

$$T = \bar{T} \quad \text{on} \quad \Gamma_1 \tag{43}$$

$$\left[\sum_{m=0}^{6} \beta_m \Lambda^{(m)}\right] \frac{\partial T}{\partial x_i} n_i = h(T - T_\infty) + e C_\delta (T^4 - T^4_\infty) \quad \text{on} \quad \Gamma_2 \tag{44}$$

where Γ_1 is related to prescribed temperature boundary and Γ_2 represents the convection–radiation boundary. Note that n_i is the normal vector component, h is the convection coefficient, e is the material emissivity and C_δ is the Stefan–Boltzman constant.

4. Cylindrical bodies

This contribution considers through hardening of cylindrical bodies as an application of the proposed general formulation. Cylindrical bodies were also considered in other references dealing with different aspects of the constitutive modeling (Silva et al., 2003, 2004, 2005). Under this assumption, heat transfer analysis may be reduced to a one-dimensional problem. Moreover, plane stress or plane strain state can be assumed. Under these assumptions, only radial, r, circumferential, θ, and longitudinal, z, components need to be considered and a one-dimensional model is formulated. For this case, tensor quantities presented in the previous section may be replaced by scalar or vector quantities. As examples, one could mention: $\sum_{m=0}^{6} \beta_m E^{(m)}_{ijkl}$ replaced by $\sum_{m=0}^{6} \beta_m E^{(m)}$; $\sum_{m=0}^{6} \beta_m H^{(m)}_{ijkl}$ replaced by $\sum_{m=0}^{6} \beta_m H^{(m)}$; σ_{ij} replaced by σ_i ($\sigma_r, \sigma_\theta, \sigma_z$). A detailed description of these simplifications can be found in Pacheco et al. (2001), Silva et al. (2004, 2005), Silva (2002) and Oliveira (2004).

The numerical procedure here proposed is based on the operator split technique (Ortiz et al., 1983; Pacheco, 1994) associated with an iterative numerical scheme in order to deal with nonlinearities in the formulation. Under this assumption, coupled governing equations are solved from four uncoupled problems: thermal, phase transformation, thermo-elastic and elastoplastic. A brief discussion of each one of these problems is presented bellow.

4.1. Thermal problem

Comprises a radial conduction problem with convection. Material properties depend on temperature, and therefore, the problem is governed by nonlinear parabolic equations. An implicit finite difference predictor-corrector procedure is used for numerical solution (Ames, 1992; Pacheco, 1994).

4.2. Phase transformation problem

The volume fractions of phases are determined in this problem. Evolution equations are integrated from a simple implicit Euler method (Ames, 1992; Nakamura, 1993).

4.3. Thermo-elastic problem

Stress and displacement fields are evaluated from temperature distribution. Numerical solution is obtained employing a shooting method (Ames, 1992; Nakamura, 1993).

4.4. Elastoplastic problem

Stress and strain fields are determined considering the plastic strain evolution in the process. Numerical solution is based on the classical return mapping algorithm (Simo and Hughes, 1998).

5. Experimental procedure

The experimental procedure consists of heating cylindrical specimens with external radius $R = 25.4$ mm = 1", made of SAE 4140H steel, above its critical temperature (830 °C), holding at that temperature for 1 h to promote the complete austenitizing of the workpiece. Afterwards, a cooling process is performed considering two different media: air and water. Four cylindrical specimens are used: one specimen with two holes (one at the cylinder center and the other at 1mm from the cylinder surface) and three other specimens with only one hole at the cylinder center. Thermocouples (type K), housed in a 1.5 mm diameter inconel cover, are introduced at each hole in order to monitor the temperature time history that is registered by a data acquisition system. An uncertainty of approximately 5 °C is expected. After the quenching process, metallographic samples are prepared by the conventional technique of manual grinding and polishing followed by chemical etching with nital 2% reagent. The characterization of the resulting microstructure is carried out by optical microscopy and the volume fraction of phases is determined by the point count technique. In the present work, a grid of 100 points is applied over 10 fields over the sample, which results in 1000 points and an uncertainty less than 5% is expected. Fig. 2 shows the furnace, the data acquisition system and a schematic picture of the cylindrical specimen (Oliveira et al., 2003; Oliveira, 2004).

5.1. Air cooling

Initially, air cooling medium is of concern. Fig. 3 presents the temperature time history curves. Fig. 3a presents the thermocouple response at the center of the specimen and also at 1 mm from the cylinder surface. On the other hand, Fig. 3b shows the response from different specimens where the thermocouple is at the center of the cylinder. It should be pointed out that, when the specimen is about 650 °C, a temperature increase can be observed. This phenomenon is related to the thermomechanical coupling (Silva et al., 2004; Denis, 1996; Woodard et al., 1999) associated with the latent heat of the austenite → pearlite phase transformation.

The microstructure at an internal cross section of the cylinder far from the edges, at three regions ($r = 0$, $r = 0.5\,R$ and $r = R$), is presented in Fig. 4. The metallographic analysis reveals a homogeneous radial phase distribution with 24% of ferrite and 76% of pearlite, as summarized in Table 1.

5.2. Water cooling

At this point, water cooling medium is of concern. This medium provides quenching conditions that are associated with great amount of matensitic formation and therefore, it is related to severe mechanical conditions. Fig. 5 presents the temperature time history curves while Fig. 6 presents

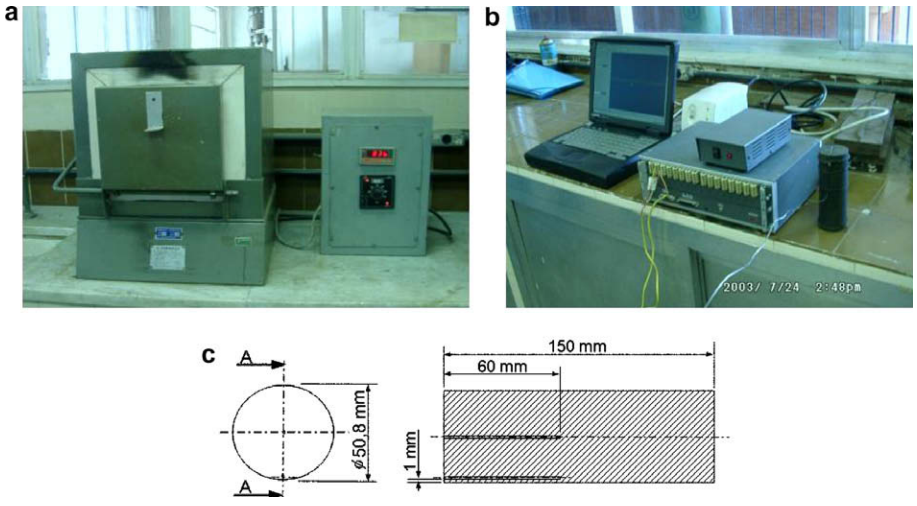

Fig. 2. (a) Furnace, (b) data acquisition system and (c) cylindrical specimen.

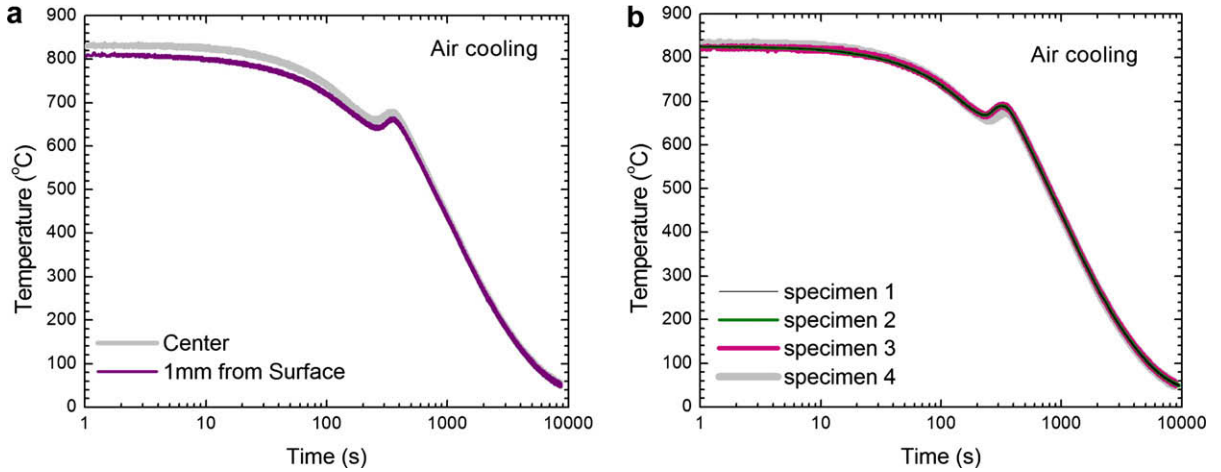

Fig. 3. Air cooling temperature evolution (a) at the center and at 1 mm from the cylinder surface and (b) temperature from four specimens measured at the cylinder center.

the metallographic analysis after the quenching process that is summarized in Table 2 presenting volume fraction phase distribution. It can be observed that martensite is predominant after this heat treatment.

6. Numerical simulations

The forthcoming analysis tries to reproduce the conditions of the experiment described in the preceding section using numerical simulations related to the proposed model for two quenching conditions: air and water cooling. Therefore, SAE 4140H steel, 25.4 mm (1") external radius cylinder is considered. Simulations consider initial conditions with homogeneous temperature and volume fraction distributions ($T = 830\ ^\circ C$ and $\beta_A = 1$).

Material parameters of the SAE 4140H steel are the following (Denis et al., 1985; Denis et al., 1999; Woodard et al., 1999; Sjöström, 1985; Melander, 1985; Oliveira, 2004): $\gamma^{(1)} = 3.333 \times 10^{-3}$, $\gamma^{(3)} = \gamma^{(4)} = \gamma^{(5)} = 5.000 \times 10^{3}$, $\gamma^{(6)} = 1.110 \times 10^{2}$, $\kappa^{(m)} = [5/(2S_Y^{(0)})]\gamma^{(m)}$ (where $S_Y^{(0)}$ is the austenite yielding stress and $m = 1, \ldots, 6$), $\rho = 7800\ kg/m^3$, $M_s = 340\ ^\circ C$, $M_f = 140^\circ C$, $e = 0.76$. Cementite parameters are not listed since this phase does not appear alone in SAE 4140H steel being part of the pearlite phase together with the ferrite phase. Other parameters that are phase and temperature dependent and, therefore, need to be interpolated from experimental data, are described by polynomial expressions. Material parameters E, c and Λ are expressed as phase and temperature dependent (Table 3–5). Although other material parameters are phase dependent by the same way, it is assumed that they are only temperature dependent in order to use experimental data furnished by other authors (Tables 6–8). Finally, Table 9 presents the convection coefficient used in simulations for two different quenching conditions: air and water cooling.

Temperature dependent parameters for diffusive phase transformations are obtained from TTT diagrams (ASM, 1977). Moreover, latent heat released associated with the enthalpy variation in a transformation process involving

Table 1
Air cooling specimen: volume fraction phase distribution.

Phase	Volume fraction (%)		
	$r = 0$	$r = 0.50R$	$r = R$
Austenite	0	0	0
Ferrite	24	24	24
Pearlite	76	76	76
Bainite	0	0	0
Martensite	0	0	0

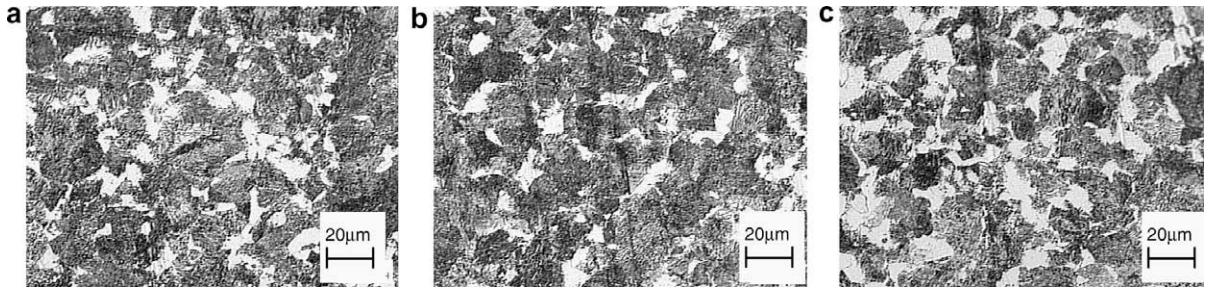

Fig. 4. Air cooling specimen microstructure: (a) center ($r = 0$), (b) $r = 0.50R$ and (c) surface ($r = R$). Etching nital 2%.

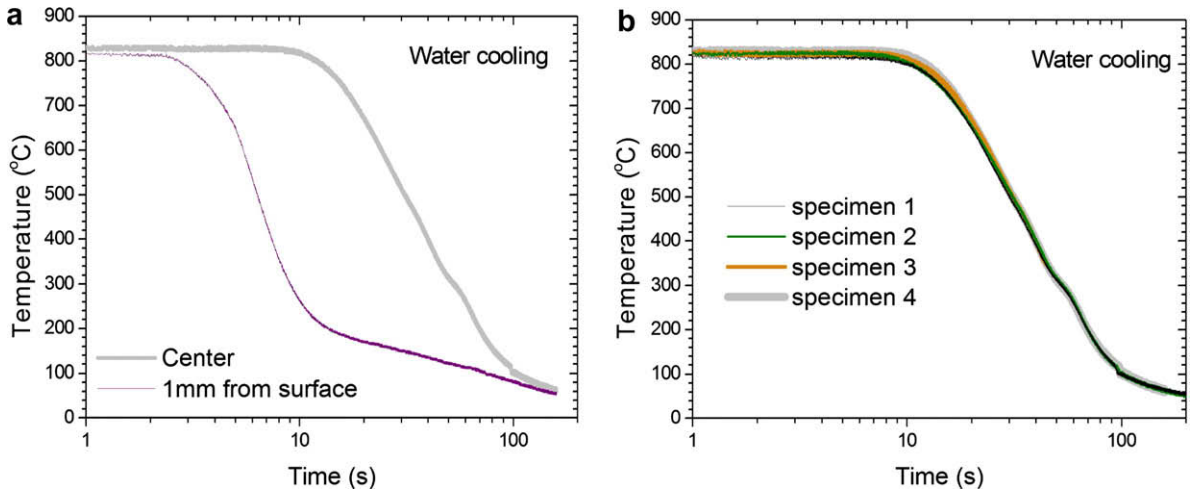

Fig. 5. (a) Temperature time history at the center and at 1 mm from the surface for the cylinders and (b) temperature time history for four specimens cooled in water.

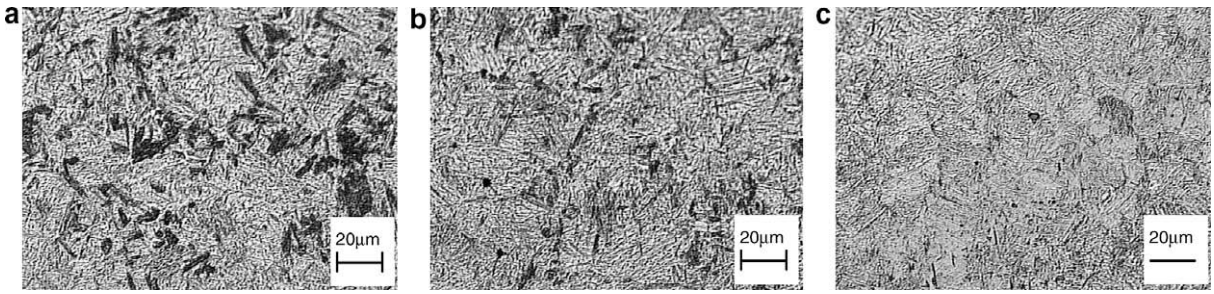

Fig. 6. Water cooling specimen microstructure: (a) center ($r = 0$), (b) $r = 0.50R$ and (c) suface ($r=R$). Etching nital 2%.

Table 2
Water cooling specimen: volume fraction phase distribution.

Phase	Volume fraction (%)		
	$r = 0$	$r = 0.50R$	$r = R$
Austenite	0	0	0
Ferrite	0	0	0
Pearlite	0	0	0
Bainite	0	0	0
Martensite	100	100	100

Table 3
Young modulus (Melander, 1985; Hildenwall, 1979; Silva et al., 2004).

Phase	E (Pa)	Temperature range
Austenite	$1.985 \times 10^{11} - 4.462 \times 10^{7}$ $T - 9.090 \times 10^{4}\, T^2 - 2.059\, T^3$	19 °C $\leqslant T \leqslant$ 900 °C
Ferrite, pearlite, upper and lower bainite, martensite	$2.145 \times 10^{11} - 3.097 \times 10^{7}$ $T - 9.208 \times 10^{4}\, T^2 - 2.797\, T^3$	19 °C $\leqslant T \leqslant$ 400 °C

a parent phase (austenite) and a product phase β_m ($m = 1, \ldots, 6$) are given in Table 10.

6.1. Air cooling

In order to compare numerical and experimental results, Fig. 7 gives the temperature distribution in two different positions: at the center and at 1 mm from the surface of the cylinder. The close agreement between the results should be noted and it is important to highlight the thermomechanical coupling effect represented by the temperature increase around 650 °C. This effect is associ-

Table 4
Specific heat (Herming et al., 1997).

Phase	ρc (Ws/m^3 °C)	Temperature range
Austenite	4.290×10^{6}	$T <$ 200°C
	$4.019 \times 10^{6} + 4.034 \times 10^{-1}$ $T^2 + 2.015 \times 10^{4}\sqrt{T}$	200 °C $\leqslant T \leqslant$ 900 °C
Ferrite, pearlite	$3.420 \times 10^{6} + 1.347 \times 10^{-1}$ $T^{2.5} - 3.745 \times 10^{-3} T^3$ $+2.698 \times 10^{-2}\sqrt{T}$	19 °C $\leqslant T \leqslant$ 900 °C
Upper and lower bainite	$3.487 \times 10^{6} + 1.404$ $\times 10^{3} T + 5.715 \times 10^{3}\sqrt{T}$	19 °C $\leqslant T \leqslant$ 600 °C
Martensite	$3.410 \times 10^{6} + 3.215$ $\times 10^{-3} T^3 + 2.919 \times 10^{4}\sqrt{T}$	19 °C $\leqslant T \leqslant$ 400 °C

Table 5
Thermal conductivity (Herming et al., 1997).

Phase	Λ (W/m °C)	Temperature range
Austenite	18	$T < 200$ °C
	$10.41 + 2.51 \times 10^{-8} T^{2.5} + 4.653 \times 10^{-1} \sqrt{T}$	200 °C $\leqslant T \leqslant$ 900 °C
Ferrite, pearlite	$44.01 - 3.863 \times 10^{-5} T^2 - 3.001 \times 10^{-7} T^{2.5}$	19 °C $\leqslant T \leqslant$ 900 °C
Upper and lower bainite	$44.04 - 4.871 \times 10^{-4} T^{1.5} - 1.794 \times 10^{-8} T^3$	19 °C $\leqslant T \leqslant$ 600 °C
Martensite	$44.05 - 5.019 \times 10^{-4} T^{1.5} - 1.611 \times 10^{-8} T^3$	19 °C $\leqslant T \leqslant$ 400 °C

Table 6
Hardening modulus (Melander, 1985; Hildenwall, 1979; Silva et al., 2004).

H (Pa)	Temperature range
$2.092 \times 10^8 + 3.833 \times 10^7 (T+273) - 3.459 \times 10^4 (T+273)^2$	20 °C < T < 450 °C
$2.259 \times 10^{11} - 2.988 \times 10^8 (T+273)$	450 °C $\leqslant T \leqslant$ 475 °C
$5.064 \times 10^9 - 3.492 \times 10^6 (T+273)$	T > 475 °C

Table 7
Yield stress (Melander, 1985; Hildenwall, 1979; Silva et al., 2004).

S_Y (Pa)	Temperature range
$7.520 \times 10^8 + 2.370 \times 10^5 (T+273) - 5.995 \times 10^2 (T+273)^2$	20 °C < T < 450 °C
$1.598 \times 10^{10} - 2.126 \times 10^7 (T+273)$	450 °C $\leqslant T \leqslant$ 475 °C
$1.595 \times 10^8 - 1.094 \times 10^5 (T+273)$	T > 475 °C

Table 8
Coefficient of linear thermal expansion (Melander, 1985; Hildenwall, 1979; Silva et al., 2004).

α_T (1/°C)	Temperature range
$1.115 \times 10^{-5} + 1.918 \times 10^{-8} T - 8.798 \times 10^{-11} T^2 + 2.043 \times 10^{-13} T^3$	20 °C < T < 475 °C
2.230×10^{-5}	T > 475 °C

ated with the latent heat of the austenite → pearlite phase transformation. In order to verify this argument, Fig. 8 presents the temperature time history for five positions of the cylinder by considering two different models: *coupled*, that considers thermomechanical coupling terms; and *uncoupled*, that neglects these terms. Note that the *uncoupled* model is not able to capture this temperature increase around 650 °C, while the coupled model captures this effect that is in agreement with experimental data.

Based on numerical simulations, the volume fraction distribution is evaluated and results are summarized in Table 11, showing again, a close agreement with experimental results presented in Table 1. The residual stress distribution along the cylinder radius is presented in Fig. 9. The determination of this stress distribution is an important information that can be extracted from the proposed constitutive model. Besides the level of stress component values, it is important to identify the presence of

Table 9
Convection coefficient (Araújo, 1982; Gür and Tekkaya, 2001).

Medium	$h\ \left(\mathrm{W/m^2}\left(\frac{J}{m^2 °C}\right)\right)$	Temperature range
Air	$8.0 \times 10^{-2} \sqrt[4]{(0.2875T - 6.0686) \times 10^6}$	19 °C $\leqslant T \leqslant$ 900 °C
Water	$4350 + 19.29T$	0°C < $T \leqslant$ 200 °C
	$4452.5 + 18.773T$	200 °C < $T \leqslant$ 400 °C
	$-8438.3 + 51T$	400 °C < $T \leqslant$ 460 °C
	$19583.57 - 14.167T$	460 °C < $T \leqslant$ 500 °C
	$31615 - 38.23T$	500 °C < $T \leqslant$ 560 °C
	$43991 - 60.33T$	560 °C < $T \leqslant$ 600 °C
	$39509 - 52.86T$	600 °C < $T \leqslant$ 700 °C
	$16996.3 - 20.699T$	700 °C < $T \leqslant$ 800 °C
	$2851.5 - 3.018T$	800 °C < $T \leqslant$ 900 °C

Table 10
Latent heat (Denis et al., 1987; Woodard et al., 1999; Stull and Prophet, 1971).

Phase transformation	ΔH (J/m^3)
Austenite → ferrite	$1.082 \times 10^2 - 0.162(T+273) + 1.118 \times 10^{-4} (T+273)^2 - 3.000 \times 10^{-8} (T+273)^3 - \frac{3.501 \times 10^4}{(T+273)}$
Austenite → pearlite, upper and lower bainite	$1.560 \times 10^9 - 1.500 \times 10^6 T$
Austenite → martensite	6.400×10^8

tensile stresses at the specimen surface that could be used for engineering purposes.

6.2. Water cooling

The quenching process with water as a cooling medium is now in focus. Temperature distributions in two different positions (at the cylinder center and at 1 mm from the cylinder surface) are presented in Fig. 10. At the center of the body there is a close agreement between numerical and experimental results. The position at 1 mm from the surface, on the other hand, presents results that capture just the general behavior. This discrepancy is explained by the thermocouple influence in the measurement. Actually, it is possible to make adjustments considering the heat conduction through the thermocouple, evaluating the temperature at its center. The finite element method may be used with this aim and the commercial finite element code ANSYS (ANSYS, 2006) is employed in order to evaluate the temperature distribution measured at the thermocouple center. Element PLANE13 is employed to study the temperature evolution of the cylinder cross-section during quenching. Symmetry conditions are employed and results are presented in Fig. 11 which shows a good agreement with experimental results.

Table 12 shows the volume fraction distribution evaluated from numerical simulation. Once again, numerical results are still in agreement with experimental data. However, simulations have predicted the presence of bainite in contrast with experimental results. Nevertheless, it is important to observe that experimental data is

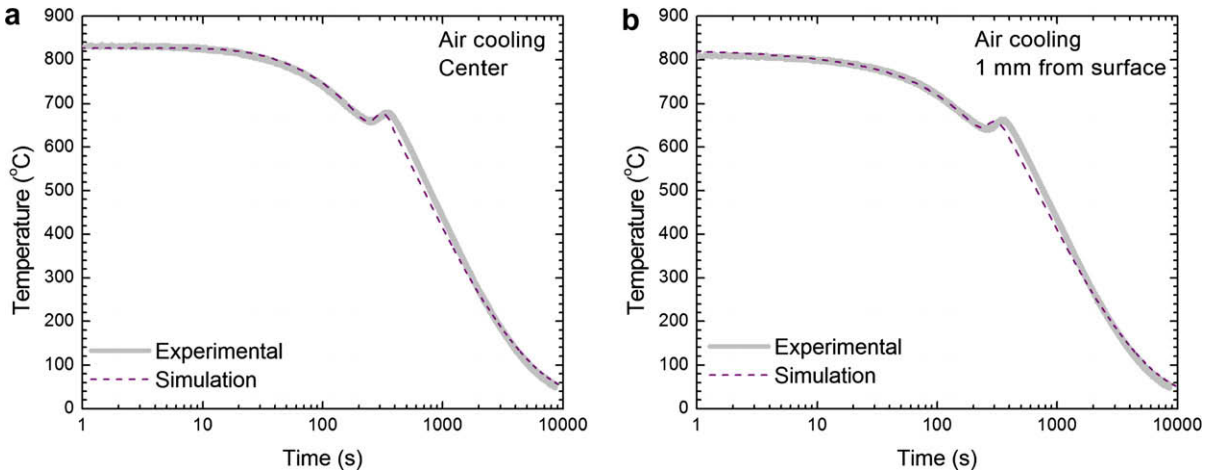

Fig. 7. Air cooling temperature time history: (a) at the center and (b) at 1 mm from the cylinder surface.

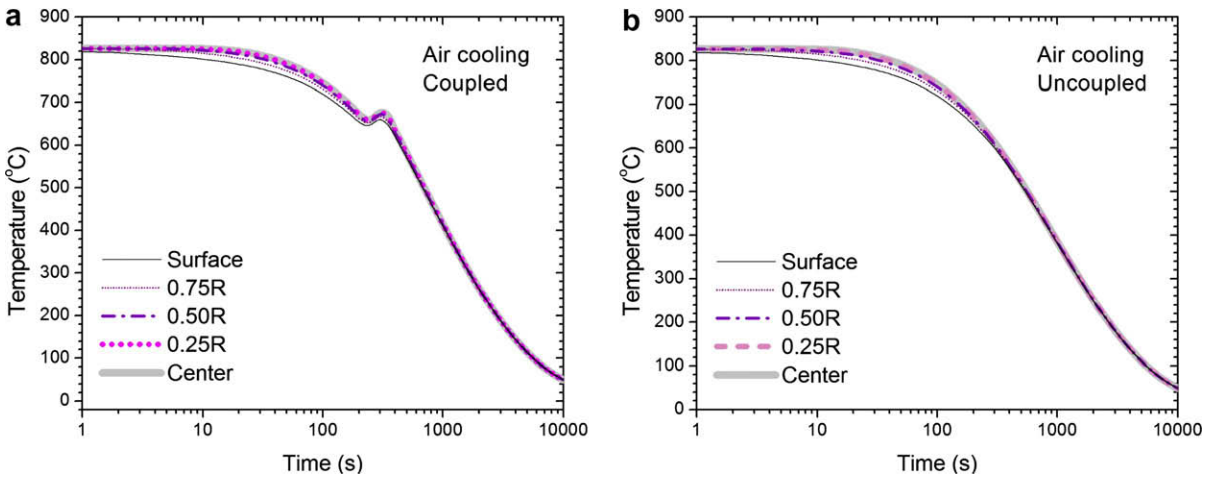

Fig. 8. Temperature time history for (a) *coupled* and (b) *uncoupled* models.

obtained by optical microscopy analysis in order to conclude the phase distribution and therefore, this difference may be less than presented.

Temperature time histories for the coupled and uncoupled models are presented in Fig. 12, for five positions of the cylinder. Results are essentially the same except for the small region close to the center of the specimen that presents a temperature increase due to thermomechanical

Table 11
Air cooling simulation: volume fraction phase distribution.

Phase	Volume fraction (%)		
	$r = 0$	$r = 0.50R$	$r = R$
Austenite	0	0	0
Ferrite	27	27	27
Pearlite	73	73	73
Bainite	0	0	0
Martensite	0	0	0

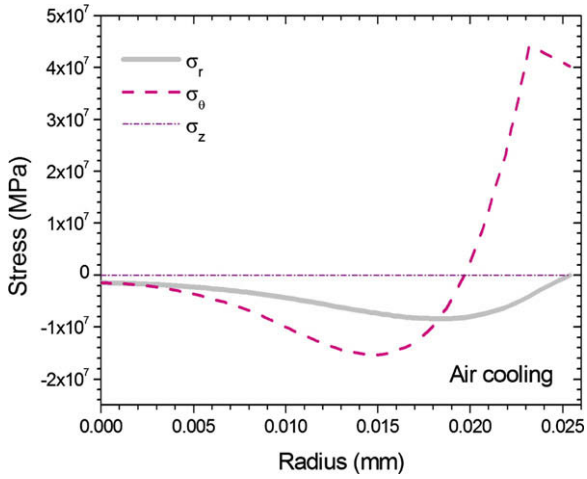

Fig. 9. Residual stress distribution for air cooling process.

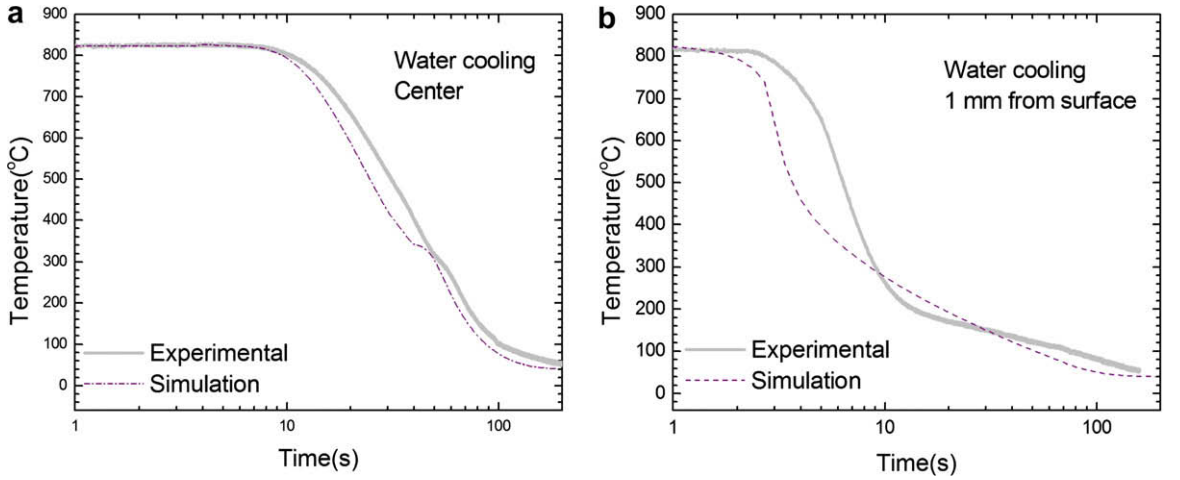

Fig. 10. Air cooling temperature time history: (a) at the center and (b) at 1 mm from the surface for the cylinders.

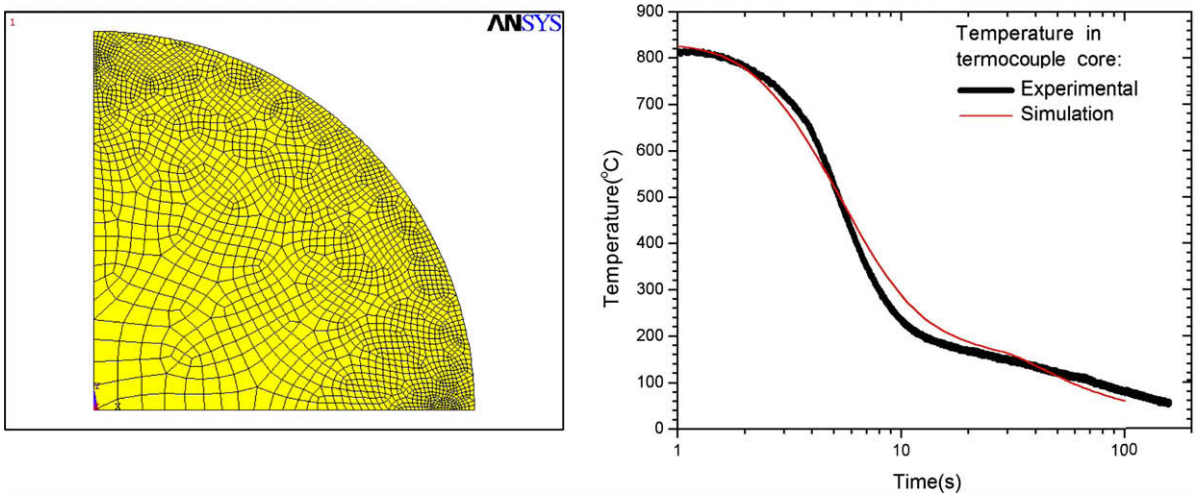

Fig. 11. Finite element simulation considering temperature at the thermocouple center.

Table 12
Water cooling simulation: volume fraction phase distribution.

Phase	Volume fraction (%)		
	$r = 0$	$r = 0.50R$	$r = R$
Austenite	0	0	0
Ferrite	0	0	0
Pearlite	0	0	0
Bainite	13	12	0
Martensite	87	88	100

coupling similar to the air cooling process. The residual stress distribution along the cylinder radius is presented in Fig. 13. Note the difference between the water cooling and the air cooling results. As expected, since water cooling is a more severe medium, the resulting stress levels are higher than those promoted by the air cooling process.

7. Conclusions

This work deals with the thermomechanical analysis of the quenching process. An experimental test is developed evaluating temperature evolution during the process and also phase distribution at the end of the process. Modeling and simulation are developed from an anisothermal multiphase constitutive model formulated within the framework of continuum mechanics and the thermodynamics of irreversible processes. A numerical procedure is developed based on the operator split technique associated with an iterative numerical scheme in order to deal with nonlinearities in the formulation. The proposed numerical procedure allows the use of traditional numerical methods. Through hardening of cylindrical bodies is considered as an application of the proposed general formulation. Numerical simulations present a good agreement with experimental data. Two different cooling media are of concern: air and

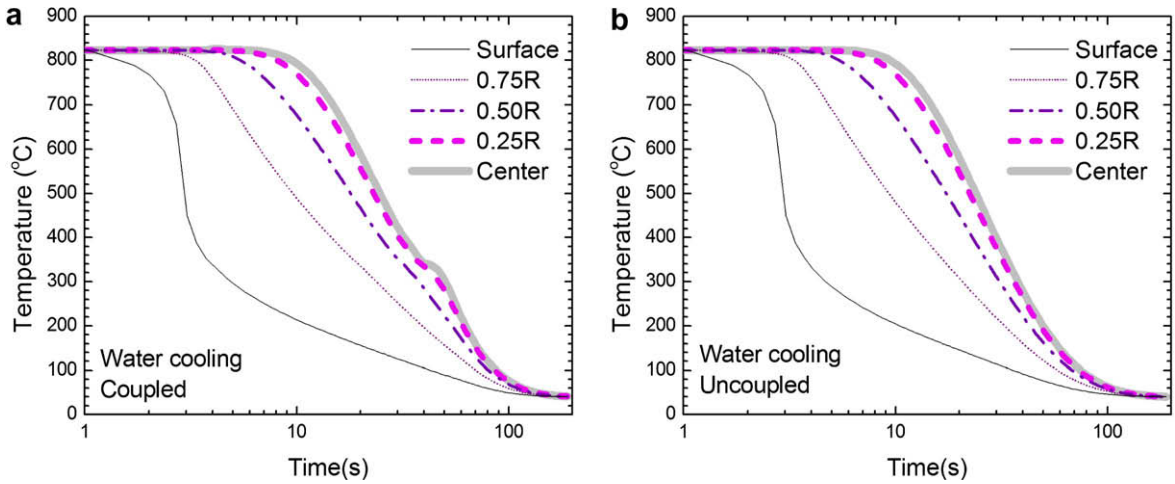

Fig. 12. Temperature time history for (a) *coupled* and (b) *uncoupled* models.

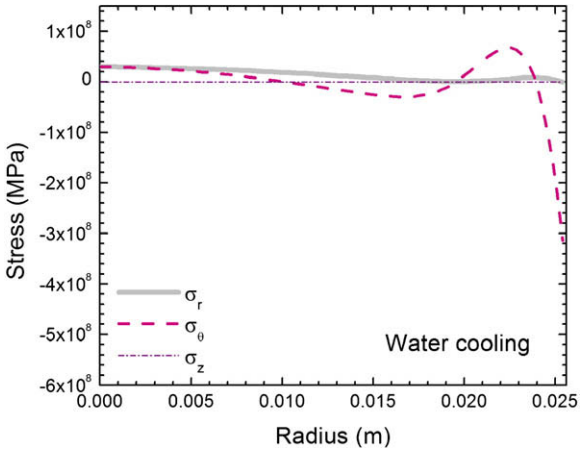

Fig. 13. Residual stress distribution for water cooling process.

water. Results related to air cooling shows that thermomechanical coupling is important being responsible to the increase in temperature during the cooling process. On the other hand, thermomechanical coupling does not have significant influence on water cooling process. Concerning phase distribution, both air and water cooling present good agreement with experimental data. Residual stresses at the end of the process are also considered. The proposed methodology can be used as a tool to study the effects of quenching parameters, as the cooling medium, and the analysis of residual stresses and phase distribution of complex geometries of quenched components.

Acknowledgements

The authors would like to acknowledge the support of the *Brazilian Research Agencies CNPq*, *CAPES* and *FAPERJ*.

References

Ames, W.F., 1992. Numerical Methods for Partial Differential Equations. Academic Press.

ANSYS, 2006, Ansys Manual, Release 9, Ansys Inc.

Araújo, C., 1982. Heat Transfer, second ed., LTC (in Portuguese).

ASM, 1977. Atlas of Isothermal Transformation and Cooling Transformation Diagrams. American Society Metals.

Avrami, M., 1940. Kinetics of phase change. II: transformation–time relations for random distribution of nuclei. Journal of Chemical Physics 8, 212.

Cahn, J.W., 1956. Transformation kinetics during continuous cooling. Acta Metallurgica 4, 572–575.

Çetinel, H., Toparl, M., Özsoyller, 2000. A finite element based prediction of the microstructural evolution of steels subjected to the tempcore process. Mechanics of Materials 32, 339–347.

Chen, J.R., Tao, Y.Q., Wang, H.G., 1997. A study on heat conduction with variable phase transformation composition during quench hardening. Journal of Materials Processing Technology 63, 554–558.

Denis, S., 1996. Considering stress-phase transformation interaction in the calculation of heat treatment residual stresses. Journal de Physique IV 6, 159–174. January.

Denis, S., Gautier, E., Simon, A., Beck, G., 1985. Stress-phase-transformation interactions – basic principles, modelling and calculation of internal stresses. Material Science and Technology 1, 805–814. October.

Denis, S., Sjöström, S., Simon, A., 1987. Coupled temperature, stress, phase transformation calculation model numerical illustration of the internal stresses evolution during cooling of a eutectoid carbon steel cylinder. Metallurgical Transactions A 18A, 1203–1212. July.

Denis, S., Archambault, S., Aubry, C., Mey, A., Louin, J.C., Simon, A., 1999. Modelling of phase transformation kinetics in steels and coupling with heat treatment residual stress predictions. Journal de Physique IV 9, 323–332. September.

Fernandes, M.B., Denis, S., Simon, A., 1985. Mathematical model coupling phase transformation and temperature evolution during quenching of steels. Materials Science and Technology 1, 838–844. October.

Gür, C.H., Tekkaya, A.E., 2001. Numerical investigation of non-homogeneous plastic deformation in quenching process. Materials Science and Engineering, 164–169.

Herming, C., Jiang, F., Honggang, W., 1997. Estimation of the mechanical properties of a 42CrMo steel cylinder with phase transformation during quenching. Journal of Materials Processing Technology 63, 568–572.

Hildenwall, B., 1979. Prediction of the Residual Stresses Created During Quenching. Ph.D. Thesis, Linkoping Univ.

Hömberg, D., 1996. A numerical simulation of the Jominy end-quench test. Acta Mater. 44 (11), 4375–4385.

Huiping, L., Guoqun, Z., Shanting, N., Chuanzhen, H., 2007. FEM simulation of quenching process and experimental verification of simulation results. Materials Science and Engineering A 452-453, 705–714.

Inoue, T., Wang, Z., 1985. Coupling between stress, temperature, and metallic structures during processes involving phase transformations. Material Science and Technology 1, 845–850.

Ju, D.Y., Zhang, W.M., Zhang, Y., 2006. Modeling and experimental verification of matensitic transformation plastic behavior in carbon

steel for quenching process. Materials Science and Engineering A, 246–250.
Kang, S.H., Im, Y.T., 2007a. Thermo-elasto-plastic finite element analysis of quenching process of carbon steel. Journal of Materials Processing Technology 192–193, 381–390.
Kang, S.H., Im, Y.T., 2007b. Three-dimensional thermo-elastic–plastic finite element modeling of quenching process of plain-carbon steel in couple with phase transformation. International Journal of Mechanical Sciences 49, 423–439.
Kang, S.H., Im, Y.T., 2007c. Finite element investigation of multi-phase transformation within carburized carbon steel. Journal of Materials Processing Technology 183, 241–248.
Koistinen, D.P., Marburger, R.E., 1959. A general equation prescribing the extent of the austenite-martensite transformation in pure iron-carbon alloys and plain carbon steels. Acta Metallurgica 7, 59–60.
Lemaitre, J., Chaboche, J.L., 1990. Mechanics of Solid Materials. Cambridge Press Univ.
Melander, M., 1985. A Computational and Experimental Investigation of Induction and Laser Hardening. Ph.D. Thesis, Department of Mechanical Eng., Linkoping University.
Nakamura, S., 1993. Applied Numerical Methods in C. Prentice-Hall.
Ortiz, M., Pinsky, P.M., Taylor, R.L., 1983. Operator split methods for the numerical solution of the elastoplastic dynamic problem. Computer Methods in Applied Mechanics and Engineering 39, 137–157.
Oliveira, W.P., Souza, L.F.G., Pacheco, P.M.C.L., Savi, M.A., 2003. Quenching Process Modeling in Steel Cylinders Using a Multi-Phase Constitutive Model. COBEM 2003 – 17th International Congress of Mechanical Engineering, São Paulo.
Oliveira, W.P., 2004. Modeling Quenching Process in Steel Cylinder Using Multi-Phase Constitutive Model. M.Sc. Dissertation, CEFET/RJ (in Portuguese).
Pacheco, P.M.C.L., 1994. Analysis of Thermomechanical Coupling in Elasto-viscous-plastic Materials, Ph.D. Thesis, Department of Mechanical Engineering, PUC-Rio.
Pacheco, P.M.C.L., Savi, M.A., Camarão, A.F., 2001. Analysis of residual stresses generated by progressive induction hardening of steel cylinders. Journal of Strain Analysis for Engineering Design 36 (5), 507–516.
Reti, T., Fried, Z., Felde, I., 2001. Computer simulation of steel quenching process using a multi-phase transformation model. Computational Materials Science 22, 261–278.
Sen, S., Aksakal, B., Ozel, A., 2000. Transient and residual thermal stresses in quenched cylindrical bodies. International Journal of Mechanical Sciences 42 (10), 2013–2029.
Silva, E.P., 2002. Modeling and Simulation of Steel Quenching Process Using Finite Element Method. M.Sc. Dissertation, Department of Mechanical and Materials Engineering, Instituto Militar de Engenharia (in Portuguese).
Silva, E.P., Pacheco, P.M.C.L., Savi, M.A., 2003. Simulation of Quenching Process Using the Finite Element Method. COBEM 2003 – 17th International Congress of Mechanical Engineering.
Silva, E.P., Pacheco, P.M.C.L., Savi, M.A., 2004. On the thermo-mechanical coupling in austenite-martensite phase transformation related to the quenching process. International Journal of Solids and Structures 41 (3-4), 1139–1155.
Silva, E.P., Pacheco, P.M.C.L., Savi, M.A., 2005. Finite element analysis of the phase transformation effect in residual stresses generated by quenching in notched steel cylinders. Journal of Strain Analysis for Engineering Design 40 (2), 151–160.
Simo, J.C., Hughes, T.J.R., 1998. Computational Inelasticity. Springer.
Sinha, V.K., Prasad, R.S., Mandal, A., Maity, J., 2007. A mathematical model to predict microstructure of heat-treated steel. Journal of Materials Engineering and Performance 16 (4), 461–469.
Sjöström, S., 1985. Interactions and constitutive models for calculating quench stresses in steel. Material Science and Technology 1, 823–829.
Sjöström, S., 1994. Physical, mathematical and numerical modelling for calculation of residual stresses: fundamentals and applications. In: Proceedings of the Fourth International Conference on Residual Stresses, June 8–10, Baltimore, USA.
Stull, D.R., Prophet, H., 1971. JANAF Thermochemical Tables, 2nd ed., National Standard Reference Data System, NSRDS-NBS 37.
Woodard, P.R., Chandrasekar, S., Yang, H.T.Y., 1999. Analysis of temperature and microstructure in the quenching of steel cylinders. Metallurgical and Materials Transactions B – Process Metallurgy and Materials Processing Science 4, 815–822. August.